THE JOURNAL OF PHYSICAL CHEMISTRY Letters

Letter

pubs.acs.org/JPCL

Time-Resolved Analysis of Domain Growth and Alignment of Cylinder-Forming Block Copolymers Confined within Nanopatterned Substrates

Hyung Ju Ryu, Qianqian Tong, and S. J. Sibener*

The James Franck Institute and Department of Chemistry, The University of Chicago, 929 East 57th Street, Chicago, Illinois, United States

Supporting Information

ABSTRACT: In this Letter, we elucidate the microstructure evolution of asymmetric poly(styrene-*b*-methyl methacrylate), PS-*b*-PMMA, block copolymer confined within nanoscale linear channels on silicon nitride substrates. We have directly observed the mechanism for cylinder alignment within the nanochannels using time-resolved AFM imaging and computerized image analysis. The overall alignment occurs via the coarsening of grains that have preferred cylinder orientation along the channel direction and is energetically driven by the interface energies of adjacent diblock domains of differing orientation. Grain coarsening is strongly affected by the annealing temperature and the geometry of the grain boundary itself. Grain coarsening promptly occurs when a domain is bordered by adjacent high-angle grain boundaries. The energetic term that drives this process arises from the fact that high-angle grain boundaries with larger excess energy migrate faster than other lower-angle grain boundaries. The velocity of grain boundary migration is proportional to the boundary tilt angle, while the activation energy depends weakly on this angle.

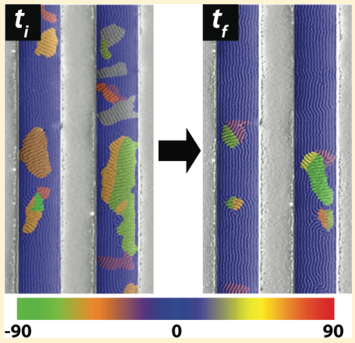

SECTION: Glasses, Colloids, Polymers, and Soft Matter

Block copolymers (BCPs), due to their unique ability to self-assemble into periodic microdomain structures, have attracted wide scientific and application-oriented interest. This has led to extensive efforts to employ dense arrays of BCP morphologies as templates for nanopatterning or functional materials.[1−10] For example, various attempts have been focused on BCP lithography in which the characteristic BCP morphologies on the length scale of tens of nanometers facilitate the fabrication of magnetic storage media, semiconductor patterns, and nanomaterials.[11−20] One of the key challenges associated with this technique is to achieve a high degree of long-range domain order in BCP structures. This has led to the development of various methods to align BCP microdomains using electric fields, flow, directional crystallization, solvent annealing, chemical patterning, and graphoepitaxy.[21−30] The main objective of these approaches has been to reduce considerably the density of defects in such BCP microstructures including dislocations, disclinations, and grain boundaries. This study offers an improved understanding of the physical chemistry of domain growth in polymeric materials and determines major parameters that govern BCP structural behavior. For this purpose, lithographic channels are utilized that impose boundary conditions in channels that template essentially perfect alignment of cylindrical BCPs in deposited thin films.

It has been well recognized that defects, which have significant impact on both long-range order and the physical properties of BCPs, are generated inherently during structure formation in BCPs.[31] Accordingly, the mechanisms of defect formation and annihilation in BCPs have been studied both experimentally and theoretically. For example, Hahm et al. examined the kinetic pathways for the evolution of one-dimensional defects, revealing the mechanisms for topological changes and mobility kinetics in thin film diblock copolymers during thermal annealing.[32,33] Also, it was demonstrated by Harrison et al. that the coarsening of cylindrical microstructures of poly(styrene-*b*-isoprene) (PS-PI) with parallel orientation to a silicon substrate occurs through the annihilation of disclinations, and the orientational correlation length grows with time as $t^{1/4}$.[34−36] Moreover, two-dimensional grain boundary (GB) defects in BCPs have been extensively explored with lamellar-forming BCPs. Gido and Thomas as well as Hashimoto first classified different types of GBs (symmetric, asymmetric tilt, and twist GBs) and examined the energetic and geometrical characteristics of those GBs in PS-PI diblock copolymers.[37−41] Subsequently, Matsen and Schick's group assessed the excessive surface energy of the three major GB types in lamellar morphologies using self-consistent field theory and/or Ginzburg−Landau theory.[42−44] However, these studies focused only on examining the features of individual GBs. Recently, Bockstaller and co-workers investigated the distribu-

Received: July 24, 2013
Accepted: August 11, 2013
Published: August 14, 2013

   dx.doi.org/10.1021/jz4015794 | *J. Phys. Chem. Lett.* 2013, 4, 2890−2895

tion of GB types in bulk lamellar PS-PI microstructures, demonstrating the relevance of the thermodynamic and kinetic features of GBs on grain coarsening during thermal annealing using serial electron imaging and subsequent image processing procedures.[31,45]

It is important to note that these previous studies were based on the static analysis of bulk materials and thus can only provide indirect evidence of structure evolution by the interpretation of the microstructures of different specimens subjected to distinct processing conditions. The objective of the present Letter is to apply time-resolved atomic force microscopy (AFM) imaging and image processing to elucidate the mechanism of structure coarsening of BCP cylinders confined within topographically patterned substrates. With this method, cylinder alignment during annealing is interpreted in terms of grain coarsening as well as the velocities of GB motion, leading to the determination of the activation energies of GB motion. From this analysis, it is demonstrated that GB migration is strongly dependent on the annealing temperature as well as the geometrical features of GBs.

Figure 1 shows a representative AFM image taken from a spin-cast cylinder-forming poly(styrene-*b*-methyl methacrylate)

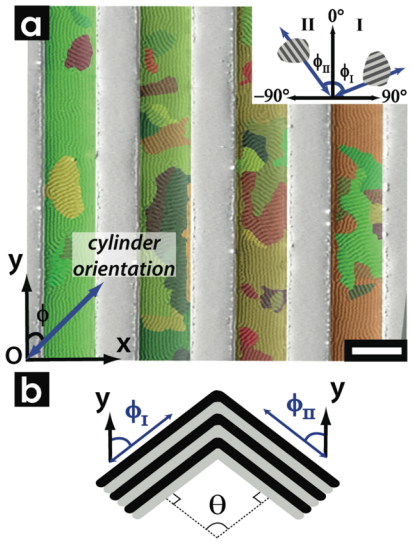

Figure 1. (a) A grain map over an AFM image of spin-cast PS-*b*-PMMA on nanopatterend Si_3N_4. The image size is 5 × 4.4 μm, and the width of each channel is 650 nm. Colors are randomly employed in these grain maps to visually clarify grain structures. The bottom-left of a selected area is defined as a coordinate origin. The inset shows the cylinder orientations of two domains with respect to the primary channel direction. The scale bar is 600 nm. (b) A schematic defining the GB tilt angle (θ), which is the intersection angle of two normal lines to cylinder orientations, ϕ_I and ϕ_{II}.

(PS-*b*-PMMA) film with 1 h of preannealing on which a grain map obtained through image processing procedures is overlaid. As shown in the figure, spin-cast polymer films in the channel show "fingerprint" patterns with only one layer of PMMA cylinders because (1) PS and PMMA have similar polymer/air interfacial energies, (2) PMMA has much lower wetting energy on Si_3N_4 than PS,[46,47] and (3) the trough depth is close to $3L/2$ (L: BCP layer thickness; this also accommodates a brush layer).[6,27,28] Image processing on AFM images is performed as follows: There are two orientation parameters utilized in this analysis. The first is cylinder orientation (ϕ) defined as the angle between the cylinders and the primary channel direction (+y-axis), as shown in Figure 1a; the range of the cylinder orientation is limited to $-90 < \phi \leq 90°$. The second is the tilt angle (θ) between two cylinder orientations of neighboring domains, which is the parameter used in our analysis. As schematically shown in Figure 1b, the GB tilt angle (θ) is defined as the intersection angle between the two normal lines drawn with respect to cylinder orientations, ϕ_I and ϕ_{II}. Then, GBs are identified when the tilt angle between adjacent grains exceeds the threshold value (the threshold is set as 15° in Figure 1a), completing a grain map, which visually describes the microstructure of the PS-*b*-PMMA thin film. A threshold is chosen between 10 and 20° to ensure identification of every GB in the structure without including false boundaries due to noise. Our results are insensitive to threshold variations within this range. Colors on the grain map of Figure 1 are randomly assigned to grains to visually illustrate the microstructure, and the bottom-left point is used as a coordinate origin for the analysis.

The structural evolution of PS-*b*-PMMA thin films on nanopatterned Si_3N_4 substrates is illustrated in Figure 2, where

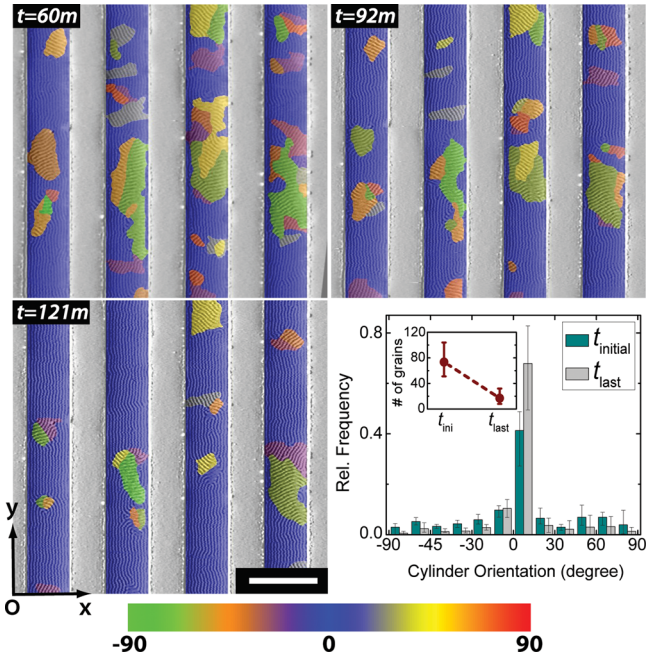

Figure 2. Illustration of the cylinder alignment during thermal annealing at 245 °C. Grain maps are overlaid on respective time-resolved AFM images. Cylinder orientations (ϕ) are depicted with scaled colors. As indicated in the color bar, green corresponds to −90°, orange to −45°, blue (along the channel direction) to 0°, yellow to 45°, and red to 90°, respectively. The scale bar indicates 1 μm. The graph shows the evolution of the distribution for cylinder orientation during thermal annealing.

respective grain maps are overlaid on time-resolved AFM images taken at 245 °C. On these grain maps, a color scale is used to indicate each grain's cylinder orientation (ϕ); as depicted in the color bar, green corresponds to a −90°, blue to a 0°, and red to a 90° cylinder orientation. It is important to note that each grain maintains its cylinder orientation during structure evolution, while grains with a cylinder orientation other than 0° diminish in size and ultimately disappear during thermal annealing through GB migration. This shows directly

dx.doi.org/10.1021/jz4015794 | J. Phys. Chem. Lett. 2013, 4, 2890−2895

that the coarsening of grains that have 0° cylinder orientation is the primary mechanism by which essentially perfect alignment of cylinders within lithographic channels is achieved, as opposed to rotation of the cylinder orientation within a given grain. In other words, due to the boundary conditions imposed by the channel, those grains having a $\phi = 0°$ cylinder orientation act as a director for domain evolution, and grow only via consumption of other grains having $\phi \neq 0$. The complete series of time-resolved AFM images taken at 245 °C, which are supplemented with overlaid grain maps, are compiled as a movie file, Movie S1 (jz4015794_si_002.mpg) with caption jz4015794_si_001.pdf, and are provided in the Supporting Information. The graph in Figure 2 represents the evolution of the number of grains and the cylinder orientation distribution during annealing at 245 °C. The analysis was performed over the total trough area of 51.3 μm^2, and the average time interval from t_{ini} to t_{last} was about 252 min. It is shown that the number of grains in a given trough area decreases while most of the cylinders become aligned parallel to the side walls. This confirms that the cylinder alignment during thermal annealing occurs primarily through enlargement of grains having the preferred orientation along the channel directions and shrinkage of grains having unfavorable alignments.

The importance of GB migration during annealing has been well-recognized in inorganic materials, and it has been known that the velocity of GB motion (v) follows

$$v = M \cdot P = M_0 \exp(-Q/RT) \cdot P \quad (1)$$

where M is the GB mobility, P the driving pressure, M_0 a mobility constant, Q the activation energy for GB migration, R the gas constant, and T the temperature.[48,49] The mobility of GBs is sensitive to parameters such as temperature, GB misorientation between adjacent grains, the orientation of GBs, and impurities segregated along GBs. The driving force for GB migration is to reduce the total free energy of the system. These forces originate from, for example, the curvature of GBs, the differences in surface or interface energies, jumps in strain energy density, and applied external fields. In this study, it is assumed that (1) the driving pressure for GB motion is from the trough walls due to the mismatch in wetting energies of PS and PMMA on Si_3N_4 substrates and (2) it is constant throughout the narrow troughs. In addition, as is well-known, the magnitude of the GB energy in BCPs is generally more than one magnitude smaller than that of the other types of interface energies.[44] Accordingly, we believe that the driving pressure from GB curvature, which is proportional to the GB energy, $P = 2\sigma_b/R$ (σ_b: GB energy; R: radius of a grain),[49] is insignificant, and the pressure from the interfacial energy mismatch, the boundary condition within the channels, is dominant. No direct relation between the velocity of GB motion (v) and the grain sizes (R) was found in our analysis. Therefore, the velocity of GB migration is presumed to be only a function of the mobility of GBs. An example of GB migration is shown in Figure 3, where the microstructure evolution of BCP cylinders during annealing at 245 °C in one trough (1.8 μm long × 0.65 μm wide) is shown; shrinking and disappearing of smaller grains with time as well as the motion of GBs is clearly illustrated in the figure. To highlight and manually measure the GB movement (the result will be shown later), five selected GBs are marked with differently colored straight lines. Because we know the precise time when each AFM image was taken and the coordinate (center of mass) of each GB with respect to the coordinate origin is given at the bottom-left, we can easily determine the velocity of each GB's motion. Here, we classify individual GBs as a function of their tilt angles (θ). Note that high-angle GBs (indicated as the yellow, green, and red lines in Figure 3) disappear earlier than others. This observation again strongly supports the notion that cylinder rotation is not the primary mechanism of cylinder alignment within the channels. Stated another way, low-angle GBs did not disappear first even though this method of evolution would have required less structural modification. The movie file, Movie S2 (jz4015794_si_003.mpg) with caption jz4015794_si_001.pdf, displaying microstructure evolution in this trough is provided in the Supporting Information.

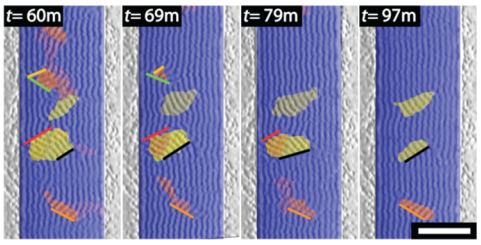

Figure 3. Illustration of GB migration during annealing. Cylinder orientations (ϕ) are presented with the same color bar as that used in Figure 2. Five GBs, indicated with five colored straight lines, are manually tracked to measure the velocity of GB motion. The scale bar corresponds to 400 nm.

Time-dependent analysis of grain maps was used to elucidate the velocities of GBs during grain coarsening. Figure 4a shows the dependence of the GB velocity on the tilt angle; in this figure, the blue symbols indicate the results from computerized analyses at 245 °C, the brown symbols are from further

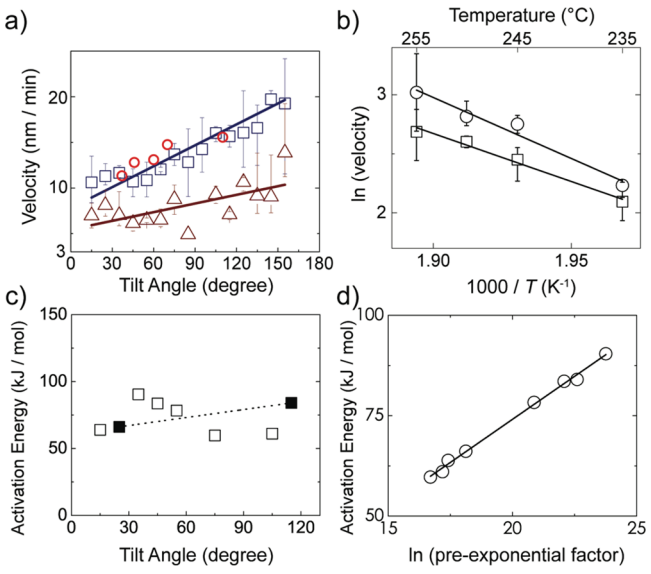

Figure 4. (a) Plot of the GB velocity as a function of the tilt angle at 235 (brown triangle) and 245 °C (blue square and red circle: manual analysis). The proportional relation between the GB velocity and tilt angle is depicted, and the straight lines are a fit to the data. (b) Arrhenius plots for two GBs with tilt angle of θ = 25 (squares) and 115° (circles). (c) Plot of the activation energy of GB migration as a function of the tilt angle. The two filled squares correspond to the two activation energies determined in panel (b). The dotted line is a visual guide. (d) Plot illustrating the dependence of the activation energy (Q) on the pre-exponential factor (A).

dx.doi.org/10.1021/jz4015794 | J. Phys. Chem. Lett. 2013, 4, 2890−2895

measurements at 235 °C, and the red symbols are from manual analysis at 245 °C. In the analysis, GB displacements were estimated between multiple time-resolved AFM images; the average velocities (in units of nm/min) for each GB's respective tilt angles were calculated with at least 50 (for high-tilt GBs) and up to 600 (for low-tilt GBs) individual measurements in order to allow for statistically meaningful sampling. Also, to confirm that the computerized analysis was not influenced by the parameter setting during image processing, the threshold angle for GB identification was varied between 10 and 20°, and all respective results fall within the error bars shown in Figure 4a. Figure 4a also reveals that the velocity of the GBs is strongly dependent on temperature as well as tilt angle. While the temperature dependence of the GB velocity can be easily understood as the mobility of GBs is a function of temperature, the implication of GB geometrical features on the velocities of GB motion is found to be rather interesting. We conjecture that the energy of tilt GBs in cylindrical BCPs increases proportionally with the tilt angle and similarly that the energy of symmetric tilt GBs continues to grow larger as the tilt angle increases until the geometrical transition of high-angle tilt GBs (Chevron) into Ω-shaped GBs (Omega) occurs in lamellar BCPs.[31,43,44] We conclude that grain coarsening in cylindrical BCPs proceeds in a way that higher free-energy GBs are promptly relieved; that is, high-angle tilt GBs migrate faster than low-angle tilt GBs. We also speculate that the Chevron to Omega transition in the lamellar structure, at which the energy of the GBs starts to level off as a function of tilt angle,[31] does not occur in cylindrical morphologies as we observe a continuous increase of the GB migration velocity as a function of the tilt angle. This is because a longer block of asymmetric polymer chains can easily stretch to fill the space along high-angle GB planes, resulting in no necessity for the geometrical transition of GBs.

From these kinetic observations, we quantitatively determined the activation energies of GB migration as a function of tilt angle using the Arrhenius relation expressed in eq 1, $\ln(v) = \ln(A) - Q/RT$, where constant M_0 and driving pressure P are both embedded into a pre-exponential factor A. Figure 4b shows the temperature dependence of the GB motion for θ = 25 and 115°, measured at 235, 245, 250, and 255 °C, from which activation energy Q (slope) and pre-exponential factor A (intercept) can be calculated. It is hard to capture the highest temperature dynamics because they align so quickly along the channel direction. Also, the measurements were done over a rather small temperature range, complicating the extraction of activation energies. Nonetheless, we include all of the data for completeness. The average activation energy for all tilt angles is determined to be ~72.8 kJ/mol, which is smaller than the one-dimensional defect diffusion activation energy in cylinder morphologies.[50] In addition, it is implied in Figure 4c that the activation energy of GB migration is weakly related to the tilt angle of GBs. It is notable that both the velocity and activation energy of GB migration are related to the GB tilt angle, which can be understood from the proportional relationship between the activation energy (Q) and pre-exponential factor (A), as shown in Figure 4d. This interdependence is referred to as the "compensation effect", which is widely recognized in thermally activated processes[51] including GB migration in metals.[52]

In summary, we have elucidated the microstructure evolution of cylinder-forming block copolymer PS-*b*-PMMA thin films on nanopatterned Si_3N_4. This has been accomplished using time-resolved AFM imaging and complementary computerized image analysis. These visualization methods have allowed us to directly observe the mechanism for PMMA cylinder alignment within topographically patterned channeled substrates. The overall alignment occurs via the coarsening of grains that have preferred cylinder orientation along the channel direction and is energetically driven by the interface energies of adjacent diblock domains of differing orientation. Quantitative analyses demonstrate that the grain coarsening is strongly affected by annealing temperature as well as by the geometrical characteristics of the GB itself, that is, grain coarsening promptly occurs when a grain is bordered by adjacent high-angle grain boundaries. The energetic term that drives this process arises from the fact that high-angle grain boundaries with larger excess energy migrate faster than other lower-angle grain boundaries. Moreover, the velocity of GB migration is proportional to the boundary tilt angle, while the activation energy depends weakly on this angle.

Our novel method of performing these studies in nanoscale linear channels provides an overall guiding field that drives the time-evolving system to essentially perfect alignment at its end point. This study furthers our understanding of microstructure evolution of cylindrical block copolymers due to thermal annealing on nanopatterned substrates, leading, ultimately, to the formation of technologically useful material platforms. It also presents a general, systematic approach by which the mechanisms responsible for GB migration in self-organizing polymeric systems can be elaborated and quantified.

■ EXPERIMENTAL SECTION

The material system used in this study consists of an asymmetric PS-*b*-PMMA with molecular weight M_w = 77 kg/mol, a polydispersity index M_w/M_n = 1.09, and a weight fraction of PMMA of 29 wt %. In a bulk state, it develops into hexagonally packed PMMA cylinders in a PS matrix with a natural layer thickness (L) of 30 nm. Thin films of this diblock copolymer were spin-cast at 5000 rpm from 0.9% toluene solutions onto topographically patterned silicon nitride (Si_3N_4) substrates and subsequently thermally annealed at 250 °C for 1 h in an argon atmosphere. The detailed description for the substrate modification is provided in ref 27, while, in this study, the silicon nitride substrates were prepared with grating patterns that contain troughs of 20 μm long, 650 nm wide, and 50 nm deep. The channel width was chosen to be the maximum that can induce perfect cylinder alignment as it allows us to separate polymer domain−domain interactions from proximal polymer−channel wall interactions in the analysis. Imaging of samples was performed using an Asylum Research MFP-3D AFM, which allows time-resolved measurements at high temperature under argon gas flow, in AC (tapping) mode using Bruker cantilevers with a spring constant of 5 N/m. The grain map was obtained by processing each AFM image with image analysis programs (using MATLAB) in such a way that first, an 8-bit gray scale image is converted to a skeletonized image and a local discrete Fourier transform is applied to every pixel on a converted image for cylinder orientation determination. Readers are referred to ref 45 and the Supporting Information, Figure S1, for further elaboration of our image processing procedures.

■ ASSOCIATED CONTENT

Supporting Information

Illustration of image processing procedures and movie files visualizing the structure evolution of BCPs during thermal

dx.doi.org/10.1021/jz4015794 | J. Phys. Chem. Lett. 2013, 4, 2890−2895

annealing. This material is available free of charge via the Internet at http://pubs.acs.org.

AUTHOR INFORMATION

Corresponding Author

*E-mail: s-sibener@uchicago.edu.

Notes

The authors declare no competing financial interest.

ACKNOWLEDGMENTS

This work was supported by DTRA under Grant No. HDTRA1-11-1-0001. It is also a pleasure to acknowledge partial support from the Materials Research Science and Engineering Center at The University of Chicago, NSF-DMR-0213745.

REFERENCES

(1) Warren, S. C.; Messina, L. C.; Slaughter, L. S.; Kamperman, M.; Zhou, Q.; Gruner, S. M.; DiSalvo, F. J.; Wiesner, U. Ordered Mesoporous Materials from Metal Nanoparticle−Block Copolymer Self-Assembly. *Science* **2008**, *320*, 1748−1752.

(2) Park, C.; Yoon, J.; Thomas, E. L. E. L. Enabling Nanotechnology with Self Assembled Block Copolymer Patterns. *Polymer* **2003**, *44*, 6725−6760.

(3) Kang, Y.; Walish, J. J.; Gorishnyy, T.; Thomas, E. L. Broad-Wavelength-Range Chemically Tunable Block-Copolymer Photonic Gels. *Nat. Mater.* **2007**, *6*, 957−960.

(4) Bockstaller, M. R.; Mickiewicz, R. A.; Thomas, E. L. Block Copolymer Nanocomposites: Perspectives for Tailored Functional Materials. *Adv. Mater.* **2005**, *17*, 1331−1349.

(5) Bockstaller, M. R.; Thomas, E. L. Proximity Effects in Self-Organized Binary Particle−Block Copolymer Blends. *Phys. Rev. Lett.* **2004**, *93*, 166106/1−166106/4.

(6) Darling, S. B.; Yufa, N. A.; Cisse, A. L.; Bader, S. D.; Sibener, S. J. Self-Organization of FePt Nanoparticles on Photochemically Modified Diblock Copolymer Templates. *Adv. Mater.* **2005**, *17*, 2446−2450.

(7) Kim, O.; Jo, G.; Park, Y. J.; Kim, S.; Park, M. J. Ion Transport Properties of Self-Assembled Polymer Electrolytes: The Role of Confinement and Interface. *J. Phys. Chem. Lett.* **2013**, *4*, 2111−2117.

(8) Lo, C.-T.; Lin, W.-T. Effect of Rod Length on the Morphology of Block Copolymer/Magnetic Nanorod Composites. *J. Phys. Chem. B* **2013**, *117*, 5261−5270.

(9) Shi, Z.; Han, M.; Song, F.; Zhou, J.; Wan, J.; Wang, G. Hierarchical Self-Assembly of Silver Nanocluster Arrays on Triblock Copolymer Templates. *J. Phys. Chem. B* **2006**, *110*, 18154−18157.

(10) Fu, Q.; Huang, S.; Liu, J. Chemical Vapor Deposition of Single-Walled Carbon Nanotubes Catalyzed by Uniform Fe_2O_3 Nanoclusters Synthesized Using Diblock Copolymer Micelles. *J. Phys. Chem. B* **2004**, *108*, 6124−6129.

(11) Park, M.; Harrison, C.; Chaikin, P. M.; Register, R. A.; Adamson, D. H. Block Copolymer Lithography: Periodic Arrays of $\sim 10^{11}$ Holes in 1 Square Centimeter. *Science* **1997**, *276*, 1401−1404.

(12) Black, C. T.; Bezencenet, O. Nanometer-Scale Pattern Registration and Alignment by Directed Diblock Copolymer Self-Assembly. *IEEE Trans. Nanotechnol.* **2004**, *3*, 412−415.

(13) Cheng, J. Y.; Ross, C. A.; Chan, V. Z.-H.; Thomas, E. L.; Lammertink, R. G. H.; Vancso, G. J. Formation of a Cobalt Magnetic Dot Array via Block Copolymer Lithography. *Adv. Mater.* **2001**, *13*, 1174−1178.

(14) Chai, J.; Wang, D.; Fan, X.; Buriak, J. M. Assembly of Aligned Linear Metallic Patterns on Silicon. *Nat. Nanotechnol.* **2007**, *2*, 500−506.

(15) Thurn-Albrecht, T.; Schotter, J.; Kastle, G. A.; Emley, N.; Shibauchi, T.; Krusin-Elbaum, L.; Guarini, K.; Black, C. T.; Tuominen, M. T.; Russell, T. P. Ultrahigh-Density Nanowire Arrays Grown in Self-Assembled Diblock Copolymer Templates. *Science* **2000**, *290*, 2126−2129.

(16) Kim, H.-C.; Jia, X.; Stafford, C. M.; Kim, D. H.; McCarthy, T. J.; Tuominen, M.; Hawker, C. J.; Russell, T. P. A Route to Nanoscopic SiO_2 Posts via Block Copolymer Templates. *Adv. Mater.* **2001**, *13*, 795−797.

(17) Peng, Q.; Tseng, Y.-C.; Darling, S. B.; Elam, J. W. Nanoscopic Patterned Materials with Tunable Dimensions via Atomic Layer Deposition on Block Copolymers. *Adv. Mater.* **2010**, *22*, 5129−5133.

(18) Tseng, Y.-C.; Peng, Q.; Ocola, L. E.; Elam, J. W.; Darling, S. B. Enhanced Block Copolymer Lithography Using Sequential Infiltration Synthesis. *J. Phys. Chem. C* **2011**, *115*, 17725−17729.

(19) Ramanathan, M.; Kilbey, S. M., II; Ji, Q.; Hill, J. P.; Ariga, K. Materials Self-Assembly and Fabrication in Confined Spaces. *J. Mater. Chem.* **2012**, *22*, 10389−10405.

(20) Selvan, S. T.; Hayakawa, T.; Nogami, M.; Moller, M. Block Copolymer Mediated Synthesis of Gold Quantum Dots and Novel Gold−Polypyrrole Nanocomposites. *J. Phys. Chem. B* **1999**, *103*, 7441−7448.

(21) Morkved, T. L.; Lu, M.; Urbas, A. M.; Ehrichs, E. E.; Jaeger, H. M.; Mansky, P.; Russell, T. P. Local Control of Microdomain Orientation in Diblock Copolymer Thin Films with Electric Fields. *Science* **1996**, *273*, 931−933.

(22) Pelletier, V.; Adamson, D. H.; Register, R. A.; Chaikin, P. M. Writing Mesoscale Patterns in Block Copolymer Thin Films through Channel Flow of a Nonsolvent Fluid. *Appl. Phys. Lett.* **2007**, *90*, 163105/1−163105/3.

(23) Park, C.; De Rosa, C.; Thomas, E. L. Large Area Orientation of Block Copolymer Microdomains in Thin Films via Directional Crystallization of a Solvent. *Macromolecules* **2001**, *34*, 2602−2606.

(24) Kim, S. H.; Misner, M. J.; Xu, T.; Kimura, M.; Russell, T. P. Highly Oriented and Ordered Arrays from Block Copolymers via Solvent Evaporation. *Adv. Mater.* **2004**, *16*, 226−231.

(25) Kim, S. O.; Solak, H. H.; Stoykovich, M. P.; Ferrier, N. J.; de Pablo, J. J.; Nealey, P. F. Epitaxial Self-Assembly of Block Copolymers on Lithographically Defined Nanopatterned Substrates. *Nature* **2003**, *424*, 411−414.

(26) Segalman, R. A.; Yokoyama, H.; Kramer, E. J. Graphoepitaxy of Spherical Domain Block Copolymer Films. *Adv. Mater.* **2001**, *13*, 1152−1155.

(27) Sundrani, D.; Darling, S. B.; Sibener, S. J. Guiding Polymers to Perfection: Macroscopic Alignment of Nanoscale Domains. *Nano Lett.* **2004**, *4*, 273−276.

(28) Sundrani, D.; Darling, S. B.; Sibener, S. J. Hierarchical Assembly and Compliance of Aligned Nanoscale Polymer Cylinders in Confinement. *Langmuir* **2004**, *20*, 5091−5099.

(29) Darling, S. B. Directing the Self-Assembly of Block Copolymers. *Prog. Polym. Sci.* **2007**, *32*, 1152−1204.

(30) Tran-Ba, K.-H.; Finley, J. J.; Higgins, D. A.; Ito, T. Single-Molecule Tracking Studies of Millimeter-Scale Cylindrical Domain Alignment in Polystyrene−Poly(ethylene oxide) Diblock Copolymer Films Induced by Solvent Vapor Penetration. *J. Phys. Chem. Lett.* **2012**, *3*, 1968−1973.

(31) Ryu, H. J.; Fortner, D. B.; Rohrer, G. S.; Bockstaller, M. R. Measuring Relative Grain-Boundary Energies in Block-Copolymer Microstructures. *Phys. Rev. Lett.* **2012**, *108*, 107801/1−107801/5.

(32) Hahm, J.; Lopes, W. A.; Jaeger, H. M.; Sibener, S. J. Defect Evolution in Ultrathin Films of Polystyrene-Block-Polymethylmethacrylate Diblock Copolymers Observed by Atomic Force Microscopy. *J. Chem. Phys.* **1998**, *109*, 10111−10114.

(33) Hahm, J.; Sibener, S. J. Time-Resolved Atomic Force Microscopy Imaging Studies of Asymmetric PS-b-PMMA Ultrathin Films: Dislocation and Disclination Transformations, Defect Mobility, and Evolution of Nanoscale Morphology. *J. Chem. Phys.* **2001**, *114*, 4730−4740.

(34) Harrison, C.; Adamson, D. H.; Cheng, Z.; Sebastian, J. M.; Sethuraman, S.; Huse, D. A.; Register, R. A.; Chaikin, P. M. Mechanisms of Ordering in Striped Patterns. *Science* **2000**, *290*, 1558−1560.

(35) Harrison, C.; Cheng, Z.; Sethuraman, S.; Huse, D. A.; Chaikin, P. M.; Vega, D. A.; Sebastian, J. M.; Register, R. A.; Adamson, D. H.

Dynamics of Pattern Coarsening in a Two-Dimensional Smectic System. *Phys. Rev. E* **2002**, *66*, 011706/1−011706/27.
(36) Harrison, C.; Angelescu, D. E.; Trawick, M.; Cheng, Z.; Huse, D. A.; Chaikin, P. M.; Vega, D. A.; Sebastian, J. M.; Register, R. A.; Adamson, D. H. Pattern Coarsening in a 2D Hexagonal System. *Europhys. Lett.* **2004**, *67*, 800−806.
(37) Gido, S. P.; Gunther, J.; Thomas, E. L.; Hoffman, D. Lamellar Diblock Copolymer Grain Boundary Morphology. 1. Twist Boundary Characterization. *Macromolecules* **1993**, *26*, 4506−4520.
(38) Gido, S. P.; Thomas, E. L. Lamellar Diblock Copolymer Grain Boundary Morphology. 2. Scherk Twist Boundary Energy Calculations. *Macromolecules* **1994**, *27*, 849−861.
(39) Gido, S. P.; Thomas, E. L. Lamellar Diblock Copolymer Grain Boundary Morphology. 4. Tilt Boundaries. *Macromolecules* **1994**, *27*, 6137−6144.
(40) Gido, S. P.; Thomas, E. L. Lamellar Diblock Copolymer Grain Boundary Morphology. 3. Helicoid Section Twist Boundary Energy. *Macromolecules* **1997**, *30*, 3739−3746.
(41) Nishikawa, Y.; Kawada, H.; Hasegawa, H.; Hashimoto, T. Grain Boundary Morphology of Lamellar Microdomains. *Acta Polym.* **1993**, *44*, 247−255.
(42) Netz, R. R.; Andelman, D.; Schick, M. Interfaces of Modulated Phases. *Phys. Rev. Lett.* **1997**, *79*, 1058−1061.
(43) Tsori, Y.; Andelman, D.; Schick, M. Defects in Lamellar Diblock Copolymers: Chevron- and Ω-Shaped Tilt Boundaries. *Phys. Rev. E* **2000**, *61*, 2848−2858.
(44) Matsen, M. W. Kink Grain Boundaries in a Block Copolymer Lamellar Phase. *J. Chem. Phys.* **1997**, *107*, 8110−8119.
(45) Ryu, H. J.; Fortner, D. B.; Lee, S.; Ferebee, R.; De Graef, M.; Misichronis, K.; Avgeropoulos, A.; Bockstaller, M. R. Role of Grain Boundary Defects During Grain Coarsening of Lamellar Block Copolymers. *Macromolecules* **2013**, *46*, 204−215.
(46) Enriquez, E. P.; Schneider, H. M.; Granick, S. PMMA Adsorption Over Previously Adsorbed PS Studied by Polarized FTIR-ATR. *J. Polym. Sci., Part B: Polym. Phys.* **1995**, *33*, 2429−2437.
(47) Morkved, T. L.; Lopes, W. A.; Hahm, J.; Sibener, S. J.; Jaeger, H. M. Silicon Nitride Membrane Substrates for the Investigation of Local Structure in Polymer Thin Films. *Polymer* **1998**, *39*, 3871−3875.
(48) Humphreys, F. J.; Hatherly, M. *Recrystallization and Related Annealing Phenomena*, 2nd ed.; Elsevier: Oxford, U.K., 2004.
(49) Gottstein, G.; Shvindlerman, L. S. *Grain Boundary Migration in Metals: Thermodynamics, Kinetics, Applications*; CRC Press: Boca Raton, FL, 2000.
(50) Ruiz, R.; Bosworth, J. K.; Black, C. T. Effect of Structural Anisotropy on the Coarsening Kinetics of Diblock Copolymer Striped Patterns. *Phys. Rev. B* **2008**, *77*, 054204/1−054204/5.
(51) Conner, W. C. A General Explanation for the Compensation Effect: The Relationship between ΔS and Activation Energy. *J. Catal.* **1982**, *78*, 238−246.
(52) Molodov, D. A.; Czubayko, U.; Gottstein, G.; Shvindlerman, L. S. Mobility of ⟨111⟩ Tilt Grain Boundaries in the Vicinity of the Special Misorientation Σ=7 in Bicrystals of Pure Aluminium. *Scr. Metall. Mater.* **1995**, *32*, 529−534.